JOURNAL OF SPACECRAFT AND ROCKETS
Vol. 39, No. 4, July–August 2002

Parametric Analysis of Fiber-Reinforced Laminated Momentum Wheel Rotors

Rania A. Hassan* and Maher Y. A. Younan†
American University in Cairo, Cairo 11511, Egypt
and
Hani A. Arafa‡ and Yehia A. Bahei-El-Din§
Cairo University, Giza 12316, Egypt

The objective is to analyze the parameters involved in the design of a graphite-reinforced-epoxy rotor that is made from axisymmetric laminated concentric rings with interferences. This design is proposed for use in a momentum wheel that is used for attitude stabilization of geosynchronous satellites. The formulation of the problem is addressed in the domain of the elasticity theory under plane stress conditions. An analytic model is developed by solving the nonhomogeneous variable-coefficients total differential equilibrium equation using the displacement formulation (Navier's approach). Four parameters of interest are investigated: the number of concentric rings, the amount of radial interferences, reinforcement volume fraction in each ring, and the lamination angle of the fibers in the hoop-radial plane with respect to the global hoop direction of the rings. The parametric analysis shows that the amount of interferences between the neighboring rings should be kept at the minimum values required to keep the rings in contact at maximum operating speeds. The analysis also proves that by increasing the amount of reinforcement volume fraction, the minimum interferences needed can be reduced proportionally. Finally, it was found that, at the required operating high speeds, the graphite fibers should be aligned in the circumferential direction and that the number of rings the rotor consists of should be kept at a minimum.

Nomenclature

C_1, C_2	=	integration constants
D	=	differential operator with respect to radial distance r
D_1	=	differential operator with respect to the dummy variable t
H	=	component (3, 3) of the global stiffness matrix
(i)	=	index for the number of the contact radius (counting from inside)
L	=	global stiffness matrix
m	=	roots of the characteristic equation of Navier's equation
N	=	number of rings of the rotor
Q	=	constant in the particular solution of the radial displacement
r	=	radial distance with respect to the global coordinate system
r_c	=	contact radius between adjacent rings
r_{in}	=	rotor inner radius
r_{out}	=	rotor outer radius
S	=	component (1, 1) of the global stiffness matrix
T	=	component (1, 2) of the global stiffness matrix
t	=	dummy variable used in the Cauchy–Euler method
u	=	radial component of displacement
u_c	=	complementary solution for the radial displacement
u_p	=	particular solution for the radial displacement
Z	=	component (2, 2) of the global stiffness matrix
z	=	axial direction of the global coordinate system
γ	=	shear strain
$\delta_{(i)}$	=	after assembly radial interference at contact radius number (i)
ε	=	normal strain
θ	=	hoop direction of the global coordinate system
ρ	=	density
σ	=	normal stress
τ	=	shear stress
ϕ	=	lamination angle with respect to the global hoop direction
ω	=	angular velocity

Introduction

GEOSTATIONARY satellites are spacecraft that are put into an equatorial orbit that is synchronous with Earth rotation about its axis; hence, they have fixed coverage areas of Earth surface. This unique characteristic makes this orbit very desirable for many services, the quality of which is directly proportional to the accuracy of the satellites in-orbit attitude. Momentum wheels are classic attitude control actuators that provide gyroscopic stiffness for the spacecraft as a means of stabilization about a single axis. Typical spacecraft platforms employ various momentum wheel combinations and configurations to control, one, two, or three axes based on mission size and attitude control requirements.

This study focuses on the design parameters of the rotor of a standard flight-proven commercial fixed momentum wheel (FMW) that is widely used in stabilizing medium size telecommunication satellites about their pitch (north/south) axes. The original design of the commercial wheel rotor uses an aluminum alloy, and the maximum speed is 5060 rpm at 55 N · m · s of angular momentum.[1–3] The limitation on the speed is dictated by the use of angular contact ball bearings that must last for the overall spacecraft orbital maneuver life (OML), which is about 13 years. Recently, magnetic bearings were introduced as an alternative to ball bearings for spacecraft components. Magnetic bearings can cope with very high speeds. Because there is no contact between the rotor and the stator, there is

Received 2 July 2001; revision received 27 December 2001; accepted for publication 30 December 2001.

*M.Sc. Student; currently Ph.D. Student, School of Aeronautics and Astronautics, Purdue University, West Lafayette, IN 47907-1282; hassanr@ecn.purdue.edu. Student Member AIAA.
†Professor of Mechanics and Design, Engineering Department.
‡Professor of Machine Design, Mechanical Design and Production Department.
§Professor of Structures, Structural Engineering Department.

no friction that would limit the lifetime of the bearings.[4] This makes it possible to use lighter wheels and higher speeds.

Alternative Design Approach for FMW Rotor

With the idea of magnetic bearings in mind, the design approach of the system under consideration would shift toward minimizing the mass of the wheel rotor while employing higher speeds to obtain ultimately the required angular momentum that is the product of the rotor polar mass moment of inertia and its operational angular velocity. The optimum solution for the lower mass objective and the high strains and stresses burden is the use of composite materials in the design of the rotor. The suggested design for the magnetically suspended momentum wheel rotor is that it be made from a number of concentric rings with interferences, as shown in Fig. 1. The innermost ring must be made from steel to provide the required interaction with the magnetic bearings. This study analyzes the behavior of the wheel when the rest of the rings are made from graphite-reinforced-epoxy (GRE) balanced angle-ply laminates.

The dimensions of the rotor are the same as those of the described FMW. The inner and outer radii are 45 and 150 mm, respectively.[1,2] The steel ring thickness is 5 mm, and the thicknesses of the rest of the laminated GRE rings are equal and are determined based on the number of the rings. With those fixed radii, and based on the density of the material used, which is a function of the reinforcement volume fraction in each ring, the depth of the rotor is determined for a specific target mass. The depth usually ranges from 9 to 15 mm for a 2-kg rotor with different reinforcement volume fractions. For an angular momentum of 55 N · m · s and for a specified total rotor mass, the mass moment of inertia is calculated, and, hence, the rotor angular speed is determined.

A closed-form mathematical formulation is derived and presented in the following section to model the behavior of the rotor under the effect of the high centrifugal forces resulting from the operational high speeds. The study first compares the performance of the suggested composite rotor vs an equivalent multiple ring rotor made from aluminum with the inner ring made from steel as well. A parametric analysis was then carried out to investigate the optimum design parameters of the GRE rotor to the application in hand. The parameters that are analyzed and optimized in the study are 1) the amount of interference between neighboring rings, 2) the fiber volume fraction in each ring, 3) the lamination angle of each ring, and 4) the number of rings.

Note that, although the analysis presented in this paper focuses on the FMW rotor design described earlier, the analytic model presented and the results shown are valid design guidelines to other applications. One other application of a rising interest in the spacecraft design community is the use of high-speed wheels as energy storage systems as opposed to classic chemical batteries that contribute in large part to the spacecraft mass (typically 10% of dry mass).[5,6]

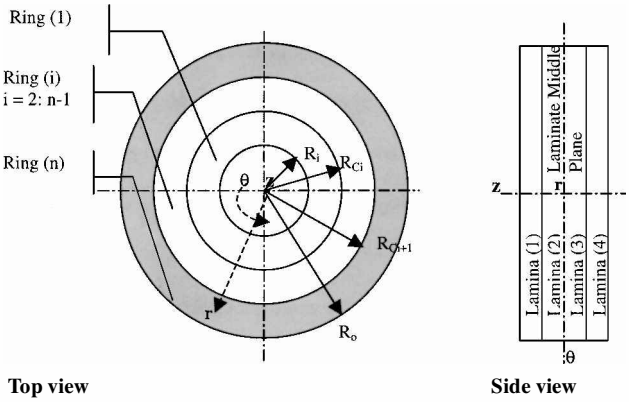

Fig. 1 Laminated *N*-ring rotor.

Analysis of Axisymmetric Laminated Concentric Rings Under Plane Stress Conditions

The analysis of the inner steel ring of the rotor or the multiple ring aluminum rotor is straightforward because it is for isotropic materials and can be found in any classical elasticity theory reference.[7] Instead, in this section, the analysis of the axisymmetric laminated rings of the GRE rotor is presented. The axisymmetry of the laminated rings means that there is no coupling between extension and twisting effects, which simplifies the analysis to a great extent as compared to the analysis of the nonaxisymmetric case.[8] There are three cases in which the laminated rings become axisymmetric with respect to the global coordinate system θ, z, and r shown in Fig. 1. For plane stress conditions, the symmetric global stiffness matrix can be reduced to 3×3 as

$$L_{\text{global}} = \begin{bmatrix} S & T & 0 \\ T & Z & 0 \\ 0 & 0 & H \end{bmatrix} \tag{1}$$

The letter symbols are arbitrary and do not represent specific elastic moduli. They are used in this form to facilitate the derivation of the solution.

There are three cases where axisymmetry occurs. First, when the lamination angle is zero, the principal material coordinate system coincides with the global coordinate system. In such a case, the fibers are aligned in the hoop direction, and S is much greater than Z. Second, when the lamination angle is 90 deg, the fibers are aligned in the radial direction. In this case, Z is much greater than S. Third, when the laminate is made from a balanced lamina $(\pm\phi \text{ deg})_s$, ϕ is the lamination angle with respect to the hoop direction. In this case,

$$S > Z \quad \text{if} \quad \phi < 45 \text{ deg} \tag{2a}$$

$$Z > S \quad \text{if} \quad \phi > 45 \text{ deg} \tag{2b}$$

$$S = Z \quad \text{if} \quad \phi = 45 \text{ deg} \tag{2c}$$

Equation (2c) is the isotropic case.

The material properties with respect to the global polar coordinate system were calculated using the Mori–Tanaka model[9] and classical lamination theory.[10] For the Mori–Tanaka model, the matrix is assumed to be isotropic, and the fibers are either isotropic or transversely isotropic.[9] In this study, the matrix is epoxy, which is an isotropic material, and the P-100 graphite fibers are transversely isotropic. The resin Young's modulus is 2.5 GPa, its Poisson's ratio is 0.4, and the approximate epoxy experimental strength is 140 MPa (Ref. 11). The elastic moduli of the transversely isotropic P-100 graphite fibers are defined in the axial plane and the transverse plane of the fibers. The axial Young's modulus is 690 GPa, and the transverse Young's modulus is 6.07 GPa. The axial plane Poisson's ratio is 0.2, the transverse plane Poisson's ratio is 0.41, and the axial plane shear modulus is 15.5 GPa (Ref. 12). The strength of the graphite P-100 fibers is assumed to be 2.2 GPa in both planes. The density used for the resin is 1810 kg/m^3 and for the fibers is 1900 kg/m^3 (Ref. 11).

The following analysis, which attempts to solve for the stresses developed due to the centrifugal effect of the angular velocity of the rotor, can be applied for any of the three specified cases. This analysis is an essential outcome of this study because it provides a closed-form exact solution for the problem at hand.

The strain–displacement relationships for the axisymmetric load and material properties under plane stress conditions reduce to hoop strain $\varepsilon_\theta = u/r$, radial strain $\varepsilon_r = \mathrm{d}u/\mathrm{d}r$, and in-plane shear strain $\gamma_{r\theta} = 0$. The stress–displacement relationships can be obtained by substituting the strain–displacement relationships into the stress–strain relationships. They can be written in a matrix form as

$$\begin{bmatrix} \sigma_\theta \\ \sigma_r \\ \tau_{r\theta} \end{bmatrix} = \begin{bmatrix} S & T & 0 \\ T & Z & 0 \\ 0 & 0 & H \end{bmatrix} \begin{bmatrix} \dfrac{u}{r} \\ \dfrac{\mathrm{d}u}{\mathrm{d}r} \\ 0 \end{bmatrix} \tag{3}$$

The equilibrium equations in polar coordinates under plane stress conditions reduce to

$$\frac{d\sigma_r}{dr} + \frac{\sigma_r - \sigma_\theta}{r} + \rho\omega^2 r = 0 \tag{4}$$

where ρ is the density of the material and ω is the angular speed of the rotor.

From Eq. (3),

$$\frac{d\sigma_r}{dr} = \frac{T}{r}\frac{du}{dr} - T\frac{u}{r^2} + Z\frac{d^2u}{dr^2} \tag{5}$$

When Eqs. (3) and (5) are substituted in Eq. (4) and simplified, Navier's equation is obtained:

$$Z\frac{d^2u}{dr^2} + Z\frac{1}{r}\frac{du}{dr} - S\frac{u}{r^2} = -\rho\omega^2 r \tag{6}$$

When both sides are multiplied by r^2/Z

$$r^2\frac{d^2u}{dr^2} + r\frac{du}{dr} - \frac{S}{Z}u = -\frac{1}{Z}\rho\omega^2 r^3 \tag{7}$$

Equation (7) is a second-order, nonhomogeneous, total differential equation with variable coefficients. To solve for the radial displacement u, the Cauchy–Euler method is used as follows. Let $r = e^t$, $du/dr = Du$, and $du/dt = D_1 u$. As proved in the Appendix,

$$r\,Du = D_1 u \tag{8a}$$

$$r^2 D^2 u = D_1(D_1 - 1)u \tag{8b}$$

When substituted in Eq. (7) and terms are collected,

$$\left(D_1^2 - \frac{S}{Z}\right)u = \frac{-1}{Z}\rho\omega^2 e^{3t} \tag{9a}$$

$$\frac{d^2u}{dt^2} - \frac{S}{Z}u = \frac{-1}{Z}\rho\omega^2 e^{3t} \tag{9b}$$

Equation (9b) is a second-order, nonhomogeneous, differential equation with constant coefficients, whose characteristic equation is

$$m^2 - S/Z = 0 \tag{10}$$

The solutions to Eq. (10) are given as

$$m = \pm\sqrt{S/Z} \tag{11}$$

The complementary solution for Eq. (9b) is

$$u_c = C_1 \exp\left(t\sqrt{S/Z}\right) + C_2 \Big/ \exp\left(t\sqrt{S/Z}\right) \tag{12}$$

Assume a particular solution $u_p = Qe^{3t}$. When differentiated twice and substituted in Eq. (9b), Q is obtained as

$$Q = -\rho\omega^2/(9Z - S) \tag{13}$$

The overall solution for the radial displacement is expressed as

$$u = C_1 \exp\left(t\sqrt{S/Z}\right) + C_2 \Big/ \exp\left(t\sqrt{S/Z}\right) - [\rho\omega^2/(9Z - S)]\exp(3t) \tag{14}$$

When the independent variable is converted back from t to r, the radial displacement is expressed as

$$u = C_1 r^{\sqrt{S/Z}} + C_2 \Big/ r^{\sqrt{S/Z}} - \rho\omega^2 r^3/(9Z - S) \tag{15}$$

When u is differentiated once and substituted into Eq. (3) and terms are collected and simplified, the stresses can be obtained as

$$\sigma_r = \left[\left(T + \sqrt{SZ}\right)r^{(\sqrt{S/Z}-1)}\right]C_1 + \left[\frac{\left(T - \sqrt{SZ}\right)}{r^{(\sqrt{S/Z}+1)}}\right]C_2 - \frac{(3Z + T)}{(9Z - S)}\rho\omega^2 r^2 \tag{16}$$

$$\sigma_\theta = \left[\left(S + T\sqrt{\frac{S}{Z}}\right)r^{(\sqrt{S/Z}-1)}\right]C_1 + \left[\frac{\left(S - T\sqrt{S/Z}\right)}{r^{(\sqrt{S/Z}+1)}}\right]C_2 - \frac{(3T + S)}{(9Z - S)}\rho\omega^2 r^2 \tag{17}$$

If there are N concentric rings, with the innermost made from steel and the rest made from a balanced laminated composite material, there will be $2N$ unknown coefficients. Equations (18) and (19) give two boundary conditions, whereas Eqs. (20) and (21) give $2N - 2$ boundary conditions. Those add up to the $2N$ boundary conditions needed to solve for the $2N$ unknown coefficients.

At r_{in},

$$\sigma_{r(1)} = 0 \tag{18}$$

At r_{out},

$$\sigma_{r(N)} = 0 \tag{19}$$

At $r_{c(i)}$,

$$\sigma_{r(i)} = \sigma_{r(i+1)} \tag{20}$$

$$\delta_{(i)} = u_{(i+1)} - u_{(i)} \tag{21}$$

A MATLAB® program was prepared to calculate the stresses and displacements generated at different angular speeds. The program consists basically of four parts. The first part calculates the overall properties of the balanced GRE laminated rings in global coordinates. The input to this part of the program is the amount of reinforcement volume fraction and the lamination angle of each ring. The second part calculates the depth and the angular speed of the rotor. In this part of the program, the inner, outer, and contact radii and the target mass of the rotor are input. When those radii and the calculated densities of each ring are used, a specific rotor depth is calculated based on the input target mass. The mass moment of inertia of the rotor is also calculated, and the required angular momentum is input to calculate the required angular speed.

The third part of the program calculates the displacements and the stresses in all rings. It starts by using the output of the first part in calculating the roots of the characteristic equations of the homogeneous part of the rings' displacements. The program then calculates the particular part of the solutions of the rings displacements. The input to this part of the program is the amount of the interferences at the five contact radii. When this input is used with the calculated speed from the second part of the program, and the boundary conditions are used, the coefficients of integration for each ring are calculated. The radial and hoop stresses and radial displacements are then calculated for each ring. The values of the radial stresses are checked at the contact radii. If they are positive, the amounts of the interferences are reinput and should be increased, and the calculations of the third part are repeated.

The last part of the program calculates the in-plane strengths of the laminated rings using the reinforcement volume fractions input in part one. Tsai–Wu failure criterion factors are then calculated. The maximum hoop stress and the radial stress at the same point are calculated from the output of part three. The factor of safety is then found by using the calculated Tsai–Wu factors and the maximum stresses.

Results

This section is divided into two main parts. The first part presents a comparison between the performance of a conventional rotor made from steel and aluminum rings and a rotor made from steel and GRE laminated rings. The second part provides the parametric analysis

of the axisymmetric laminated concentric rings variables including reinforcement volume fraction, lamination angle, amount of the interferences, and number of laminated rings.

The objective of this study is to investigate the effect of the major design parameters on the overall performance of the momentum wheel and to establish some trends that can be used as general design guidelines in a more formal design process. Because the analysis outlined in the preceding section gives a closed-form solution for the displacements and the stresses in the rotor due to the centrifugal loading, a calculus-based optimization approach can be used to optimize the rotor performance by selecting optimum design parameters. However, modern pseudo-optimization techniques, such as genetic algorithms, are more suited to this problem because it involves both continuous and discrete variables. The continuous design parameters in this problem are fiber volume fractions, interferences, and lamination angles, whereas the only discrete variable is the number of rings.

Jeong et al.[13] attempted to optimize formally the design of an energy storage flywheel and they used sequential linear programming with a line search method for the optimization algorithm. In this work, Jeong et al. did not handle the discrete variable of the number of rings and they only addressed the lamination angle and the amounts of interferences as design variables, with the fiber volume fraction and the number of rings treated as constants.[13]

Comparison Between Aluminum and GRE in Rotor Design

The first and simplest comparison to be made is to set the same design parameters for both cases (aluminum and GRE) and to compare the stresses, strains, or displacements in each case. If the rotor is made from one steel ring and five aluminum or GRE rings, and the mass is fixed to be 2 kg, the angular speed in such a case should be 25,641 rpm, which gives the required output momentum of 55 N · m · s. The geometry is also the same; the inner, contact, and outer radii are 45, 50, 70, 90, 110, 130, and 150 mm, respectively. The depth of the aluminum rotor is 10.99 mm. Two reinforcement volume fractions in the GRE case are used, 30 and 60%, for all five rings. For a volume fraction of 60% graphite, the GRE rotor is 15.527 mm deep, and for a volume fraction of 30% graphite, the GRE rotor is 15.734 mm deep. To compare the performance of the two materials, the lamination angle used is zero, which means that the fibers are aligned in the hoop direction. The interferences between the rings are designed such that the contact normal pressure at the interfaces between the five rings under study (aluminum or GRE) is very small, just to guarantee contact between the rings at the operating speed considered. The contact normal pressure that is used to keep the rings in contact at all times is about −0.5 MPa.

The after-assembly values of the interferences needed for each case, the resulting hoop stresses and radial displacement, are then compared for evaluation. The radial stress distributions of the three materials are shown in Fig. 2. The after-assembly interferences

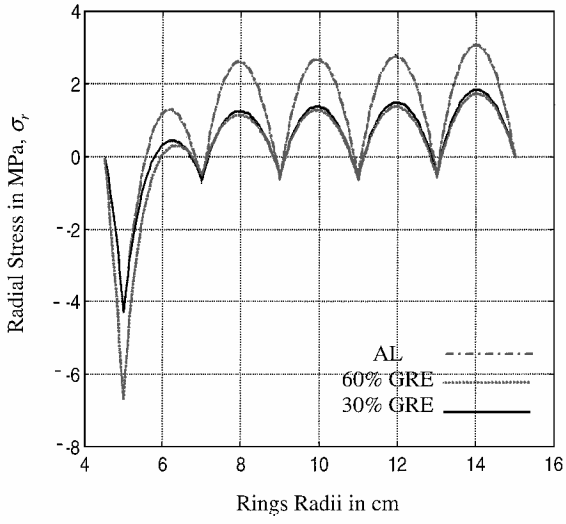

Fig. 2 Radial stress in a six-ring rotor with minimal interferences at 25,641 rpm.

Table 1 Comparative amounts of interferences for a six-ring rotor

Interference, mm	Al	60% GRE	30% GRE
2	0.0850	0.0080	0.0175
3	0.1517	0.0150	0.0310
4	0.2270	0.0240	0.0490
5	0.3227	0.0350	0.0700

Table 2 Comparative amounts of maximum hoop stresses at different speeds

	Hoop stress, MPa	
Speed (rpm)	50%	Al
5,000	12	18
10,000	43	65
15,000	100	150
20,000	170	260

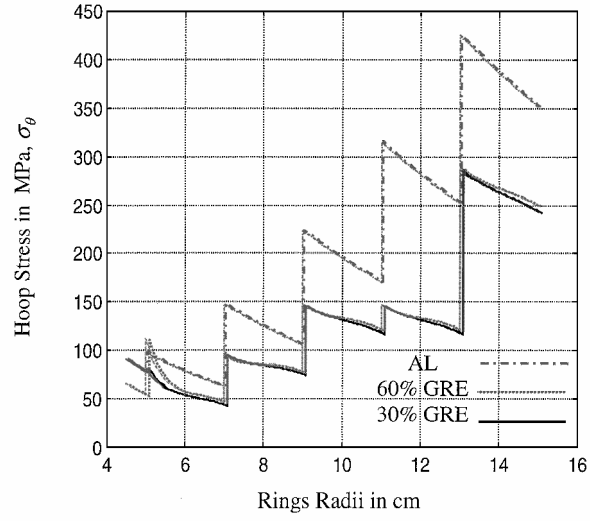

Fig. 3 Hoop stress in a six-ring rotor with minimal interferences at 25,641 rpm.

required to attain such radial stress distributions are shown in Table 1. Note that, in terms of performance, based on radial stress distribution, the after-assembly interferences required for the aluminum rings are on the average 5 times those required for the 30% GRE rings, and 10 times those required for the 60% GRE rings.

The hoop stress distribution associated with the interferences shown in Table 1 is shown in Fig. 3. It can be seen that the hoop stress in the aluminum case reaches 425 MPa in the outermost ring, whereas the hoop stress is only 275 MPa at the same point for the 30 and 60% GRE cases. Note that, at this speed, the aluminum rotor would start yielding at the outermost contact surface. That is because the aluminum yield strength is about 410 MPa (aluminum alloy 2014-T6) (Ref. 11). The radial displacements for the three cases indicate that the maximum radial displacement of the aluminum rotor exceeds by four times that of the 30% GRE rotor and by eight times that of the 60% GRE rotor.

Another comparative point of interest, which shows the advantage of using GRE over conventional aluminum rotors, is the resulting maximum hoop stress in both rotors at same speeds. For this comparative analysis, 50% reinforcement volume fraction is used with a lamination angle of zero for all of the GRE rings. For both the aluminum as well as the GRE rotors, a 2-kg mass rotor is again used. Table 2 shows the comparative maximum hoop stresses in each rotor at speeds of 5000, 10,000, 15,000, and 20,000 rpm, with the implementation of minimal interferences strategy. This strategy is ensured by selecting the amount of interferences that makes the radial stresses not decrease below −0.5 MPa at the contact surfaces. It can be observed that, at all of the investigated speeds in Table 2, the maximum hoop stresses developed in the aluminum rings rotor

are approximately 1.5 times those developed in the 50% GRE rings rotor, which is a result of the high stiffness of the graphite fibers.

The amounts of the interferences that are used to attain the behavior shown in Table 2 are much higher for the aluminum rings rotor than those needed for the 50% GRE rings rotor. It was found that the amount of interferences needed for the aluminum rotor at the speeds of 10,000, 15,000, and 20,000 rpm are on the average 7.6 times those needed for the GRE rotor.

One final point of comparison between an aluminum rotor and the 50% GRE rotor is the maximum speed each one can reach at a safety factor close to unity, that is, the speed each can reach before failure. The failure criterion used for the isotropic aluminum rotor is the von Mises criterion; whereas, for the GRE rotor, the Tsai–Wu criterion is applied. It was found that, for a safety factor of 1.04, the maximum speed the aluminum rings rotor can reach is 25,000 rpm, whereas the 50% GRE rings rotor can reach up to 45,000 rpm. To reach 25,000 rpm, the aluminum rotor needs around 2.6 times the amount of interference used for the GRE rotor at 45,000 rpm.

Parametric Analysis of Multiring GRE Rotor Design Variables

In this section, four parameters of the axisymmetric laminated rings rotor are investigated. These are the amount of the interferences, reinforcement volume fraction, lamination angle, and number of laminated rings.

Effect of Amount of Interferences

The amount of the interferences between neighboring rings is an important element in determining the stress distribution in the rotor. Two main criteria in allocating the amount of the interferences are investigated: The first is using equal amounts of interferences at all interfaces, and the second is using larger amounts of interferences at larger contact radii. For both criteria, two precautions have to be taken. First, it is important to make sure that the amount of interference chosen at any interface would keep the rings in contact at the maximum operating speed of the rotor. Second, because the interferences between the rings are going to be created by shrink-fitting the rings, it is important to check that the amount of the interferences chosen can be created by heating the rings to a temperature well below the damage temperature of the resin, which is 180°C (Ref. 11).

The first criterion in allocating the amounts of interferences between the rings is to use equal interferences. Figure 4 shows the radial stress distribution of the one steel ring and five GRE rings with 0-deg lamination angle and 60% reinforcement 2-kg rotor using equal interferences at the five interfaces. Three amounts of equal interferences were used: 0.1, 0.06, and 0.03 mm. Notice that for the 0.03-mm interference, at a speed of 25,641 rpm, σ_r at the interface between rings 5 and 6 is approximately equal to zero. This means that they are about to leave each other; therefore, this is the minimum interference that can be used.

The hoop stress distributions associated with the chosen interferences are shown in Fig. 5. It is obvious that for smaller interferences, the rotor hoop stress profile is much smoother. By decreasing the interferences from 0.1 to 0.03 mm, the maximum tensile stress of the outer ring decreased from 310 to 240 MPa, and the compressive hoop stresses in the inner steel ring went from −250 to only −35 MPa. The radial displacements for the three cases also proved the same behavior. Therefore, it is advised to use minimum interferences that would just keep the rings in contact at maximum operating speeds.

The second criterion of allocating the amounts of interferences is to increase them gradually as the contact radii increase. The main problem with this criterion is that this increase should be done based on the idea that minimum contact pressures are kept; hence, the minimum amounts of interferences are found by trial and error. Such a radial stress distribution is shown in Fig. 2. For the one steel ring and 60% 0-deg angle GRE five-ring 2-kg rotor operating at 25,641 rpm, the minimum required interferences are 0.0001, 0.0075, 0.0148, 0.0235, and 0.345 mm from innermost to outermost interface, respectively. Figure 6 compares the hoop stresses resulting from those variable interferences to the hoop stresses resulting from using a constant interference of 0.03 mm at all interfaces. This is the minimum amount of equal interferences that can keep all of the rings in contact at this operating speed.

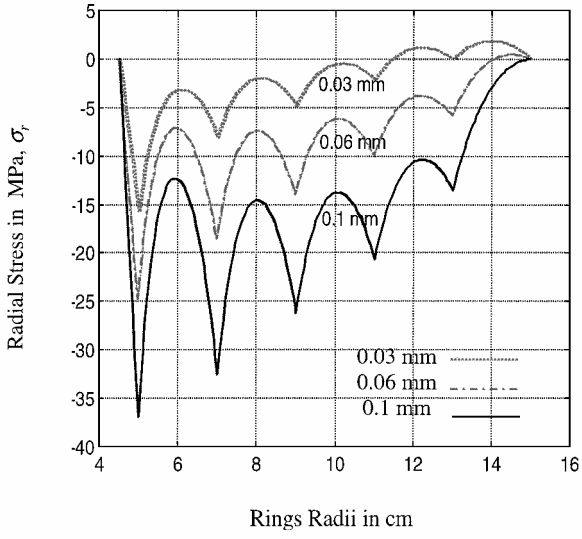

Fig. 4 Radial stress in a six-ring rotor using different values of equal interferences.

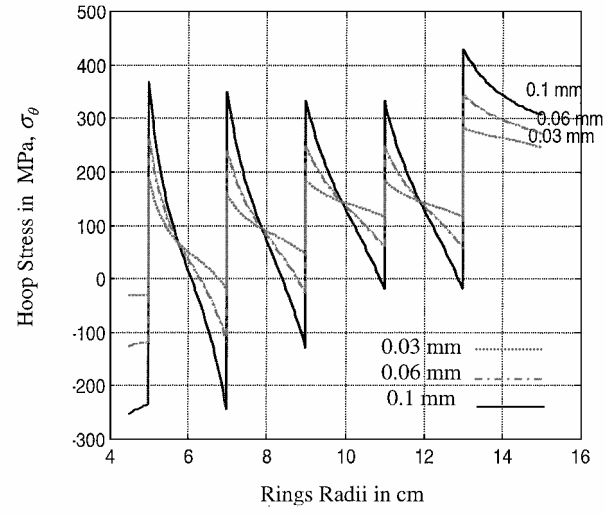

Fig. 5 Hoop stress in a six-ring rotor using different values of equal interferences.

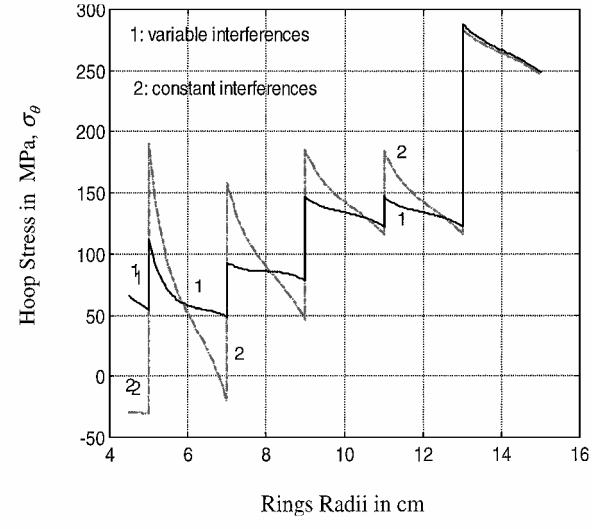

Fig. 6 Hoop stress in a six-ring rotor at 25,641 rpm.

Effect of Reinforcement Volume Fraction

An increase in the reinforcement volume fraction results in an increase in the overall material elastic moduli and strength, which means that the material is not only stiffer against forces acting on it, but it also can withstand higher stresses. To demonstrate the advantages of increasing the reinforcement volume fraction, using the strategy of equal interferences, the radial and hoop stress distributions of 60% GRE with interference of 0.03 and 0.06 mm at all interfaces and 30% GRE with interferences of 0.06 mm at all interfaces are shown in Figs. 7 and 8, respectively. Notice that, for the half reinforcement volume fraction, double the amount of interferences is needed. It can also be observed that for the case of 60% GRE with interferences of 0.06 mm, the material is overstressed.

When the variable interferences strategy (minimum contact pressure) is used for the 30 and 60% GRE, the same radial and hoop stress distributions are obtained for interferences of 0.0001, 0.0175, 0.031, 0.049, and 0.07 mm for the 30% GRE and 0.0001, 0.008, 0.015, 0.024, and 0.035 mm for the 60% GRE. Notice again that the amounts of the last three interferences of the 30% GRE rotor are double those needed for the 60% GRE rotor.

A very important point of comparison is the factor of safety (FS) associated with using both volume fractions in the design of the rotor. Using Tsai–Wu failure criterion, it was found that in the case of the 30% GRE rotor, the FS is 1.48 for both types of interference strategies, whereas, for the 60% GRE, the FS is 2.61 for both types of interference strategies.

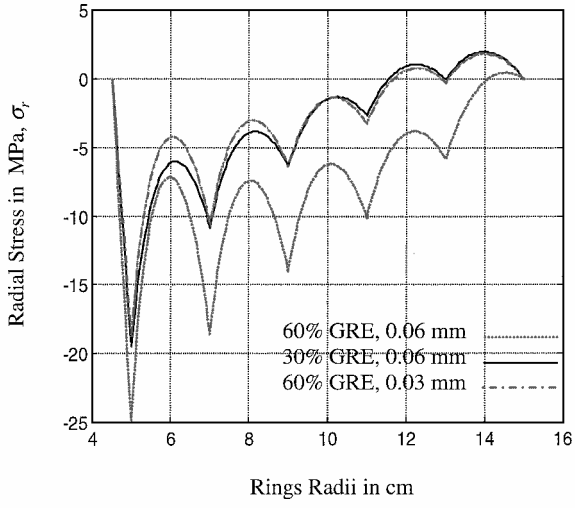

Fig. 7 Radial stress in a six-ring rotor with 60 and 30% GRE (equal interferences).

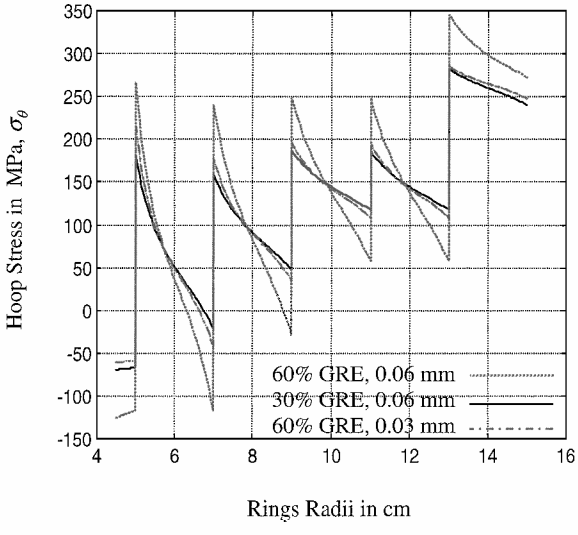

Fig. 8 Hoop stress in a six-ring rotor with 60 and 30% GRE (equal interferences).

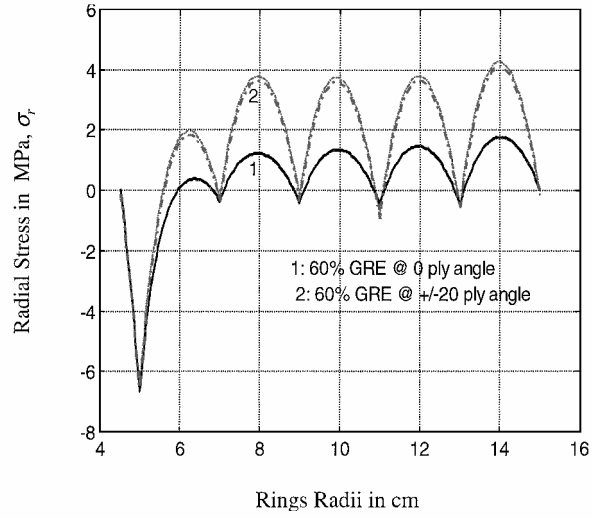

Fig. 9 Radial stress in a six-ring rotor at 25,641 rpm.

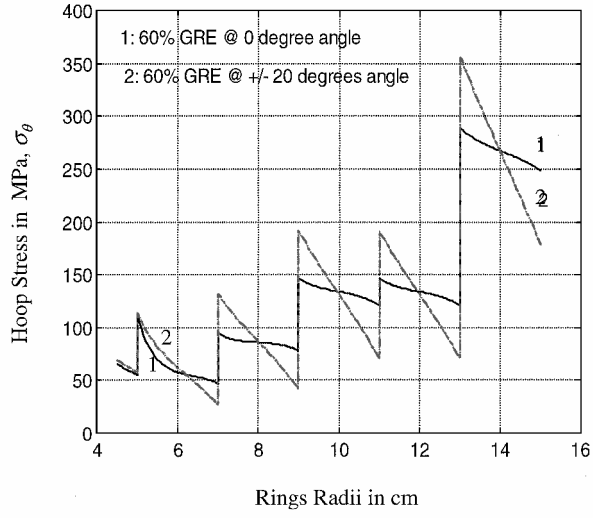

Fig. 10 Hoop stress in a six-ring rotor at 25,641 rpm.

Effect of Lamination Angle

Theoretically, the lamination angle could vary from 0 deg, which is the case when the fibers are perfectly aligned in the hoop direction, to 90 deg, which is the case where the fibers are aligned in the radial direction. The authors did not investigate the manufacturing processes that can be used to place the fibers at an angle with respect to the global hoop direction in the radial-hoop plane. Tutuncu suggests[14] that the manufacturing of this kind of reinforced laminates requires that the reinforcements be curved in the shape of a logarithmic spiral. He also points out that some materials are naturally shaped in this fashion, such as certain types of wood.

Figure 9 shows the radial stress distribution of a 60% GRE at 0-deg ply angle and at ±20-deg ply angle (balanced laminate). The interferences needed for the ±20-deg laminated rotor is six times those needed for the 0-deg laminated rotor. Figure 10 shows that the maximum hoop stress for the ±20-deg ply angle laminates exceeds that of the 0-deg ply angle laminates by 75 MPa. Furthermore, the hoop stress distribution for the 0-deg ply angle laminates is more uniform in the inner rings. Consequently, it can be concluded that, for such an application, the fibers should be aligned in the hoop direction to increase the stiffness in that direction to minimize the high stresses resulting from the centrifugal effect.

Effect of Number of Laminated Rings

For the same inner and outer radii, the rotor can be divided into only one inner steel ring and one axisymmetric GRE laminated ring, or one steel ring and a number of axisymmetric GRE laminated rings. The rationale behind dividing the laminated ring into a number

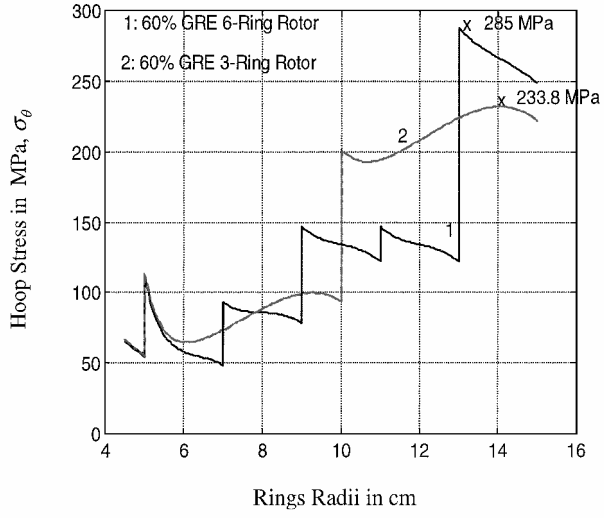

Fig. 11 Hoop stress in three-ring and six-ring rotors at 25,641 rpm.

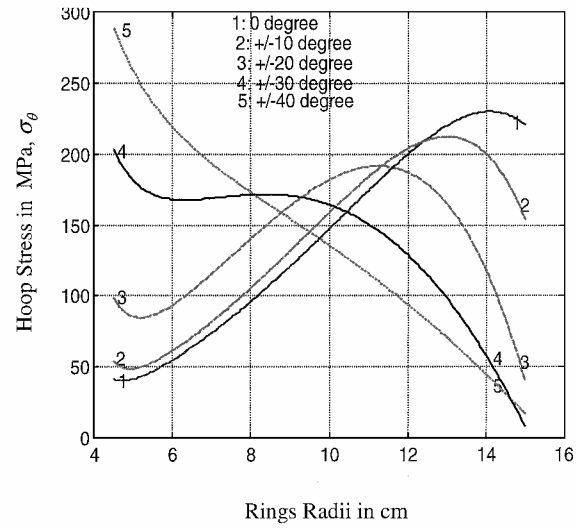

Fig. 12 Hoop stress in a one-ring rotor with different lamination angles.

of rings is to create interferences between the rings, which help in reducing the high hoop stresses induced from the high angular speed of the rotor. This technique allows also for variation of reinforcement volume fraction and lamination angle from one ring to another. The laminated part of the rotor is studied when it is composed of two and five rings. The interferences needed for the three-ring rotor are 0.0001 and 0.026 mm at inner and outer contact radii, respectively, at an angular speed of 25,641 rpm. The interferences needed for the six-ring rotor are 0.0001, 0.0075, 0.0148, 0.0235, and 0.0345 mm at contact radii starting from the innermost one.

It was found that the maximum hoop stress for the six-ring rotor is 22% higher than that of the three-ring rotor, as shown in Fig. 11, whereas the maximum radial displacement of the six-ring rotor is 12.5% higher than that of the three-ring rotor. At this speed, the FS for the six-ring rotor is 2.6, whereas it is 2.7 for the three-ring rotor. Although the idea to use shrink-fitted rings has a favorable impact on significantly decreasing the hoop stresses in the inner rings, the outer ring always suffers from exaggerated stresses. The body force increases the hoop stress by a factor of r^2 as r increases, as shown in Eq. (12); therefore, the outer points suffer from higher stresses than the inner ones. When shrink fits are employed the maximum hoop stresses of the inner rings that occur at the outer radii of the rings are reduced by the compressive prestresses produced by the fits. However, the tensile stress produced by the shrink fits at the inner radius of the outermost ring increases the overall tensile hoop stress, which is already high because of its distance from the center. Based on this analysis, it can be concluded that the fewer rings used, the less the maximum hoop stress becomes.

The conclusion that a fewer number of rings will minimize the maximum hoop stress opposes the suggestion of Kirk et al. to use a larger number of shrink-fitted rings to attain higher speeds to improve the performance of a magnetically suspended rotor used for an energy storage system.[5] Kirk et al. only suggest that the use of "interference assembled composite material rings" will help attain high speeds without providing any trade studies that support the aforementioned claim. However, in Ref. 5, Ref. 15 is referred to support the optimality of the multirim rotor design solution. In Ref. 15, Kirk investigated the best rotor shape that will maximize the energy density for an energy storage flywheel. The results show that, although a multirim rotor performance exceeds those of other suggested rotor geometries, the best performance is that of a single-ring rotor.[15]

The proposal of Jeong et al.[13] for a similar rotor design, which suggests the use of 10 concentric rings for a rotor with inner and outer radii of 50 and 100 mm, respectively, indicates that the prestress developed by using larger number of rings with interferences decreases the overall stresses in the rotor. In that study, Jeong et al.[13] only studied a 10-ring rotor, and they attempted to optimize the rotor design variables such as angular velocity, ply angles, and amount of interferences. Jeong et al. did not prove the claim that a higher number of rings will improve the rotor performance.[13]

The hoop stress distribution of the three-ring rotor shown in Fig. 11 indicates that the behavior of an axisymmetric laminate with the angular speed as the only loading is different from that of an isotropic material. The difference in the behavior between the axisymmetric laminated material and that of an isotropic material is clearly shown in Fig. 11. In the laminated material case, the maximum hoop stress occurs at a point close to the outer radius of the outer ring. For an isotropic material, the hoop stress is always maximum at the inner radius. The behavior of the axisymmetric laminate is clear in the three-ring rotor, although it is not in the six-ring rotor, which might be misleading; however, it can be justified. Note that, for the three-ring rotor, the hoop stress is high at the inner radii of both the axisymmetric rings (rings 2 and 3) because of the interference applied. The hoop stress then decreases for part of the radii and then goes to a maximum at a point close to the outer radii. For the six-ring rotor, because the rings have shorter radii, the interferences occur at points in the regions where the hoop stresses are decreasing before they increase again; therefore, this phenomenon is not observed in the six-ring rotor.

When the preceding observation is made, it is important to understand the behavior of an axisymmetric laminate under centrifugal force loading without interferences to reach an optimized design for the rotor. Figure 12 shows the hoop stress distributions of a one axisymmetric ring rotor with five different lamination angles: 0 deg, $(\pm 10\ \text{deg})_s$, $(\pm 20\ \text{deg})_s$, $(\pm 30\ \text{deg})_s$, and $(\pm 40\ \text{deg})_s$. The rotor mass is 2 kg, and it rotates at 25,641 rpm.

Note that the lowest maximum hoop stress occurs in the $(\pm 20\ \text{deg})_s$ axisymmetric laminate, and it is equal to 185 MPa. Note, also, that for the 0-deg and $(\pm 10\ \text{deg})_s$ axisymmetric laminates, the hoop stresses are maximum at a point close to the outer radius of the ring. For the $(\pm 30\ \text{deg})_s$ and $(\pm 40\ \text{deg})_s$ axisymmetric laminates, the hoop stresses are maximum at the inner radius of the ring. The hoop stress distribution for the $(\pm 40\ \text{deg})_s$ axisymmetric laminated ring is very close to that of an isotropic material; that is because, at this angle, the material is nearly isotropic in behavior because Young's modulus in the hoop direction is close to that in the radial direction. For a $(\pm 45\ \text{deg})_s$ axisymmetric laminate, the two moduli are equal.

Proposed Design Parameters for the FMW Rotor

Based on the results presented in the preceding sections, a suggested design is proposed for the FMW rotor that would be coupled with the magnetic bearings to fulfill the 55-N · m · s angular momentum storage requirement. The optimum solution for the application of the FMW rotor is the axisymmetric laminated rotor.

The suggested rotor design consists of two concentric rings of an inner radius of 45 mm and an outer radius of 150 mm. The inner ring is made from steel, and the outer one is made from 70% unidirectional GRE laminate. The reinforcement is oriented in the

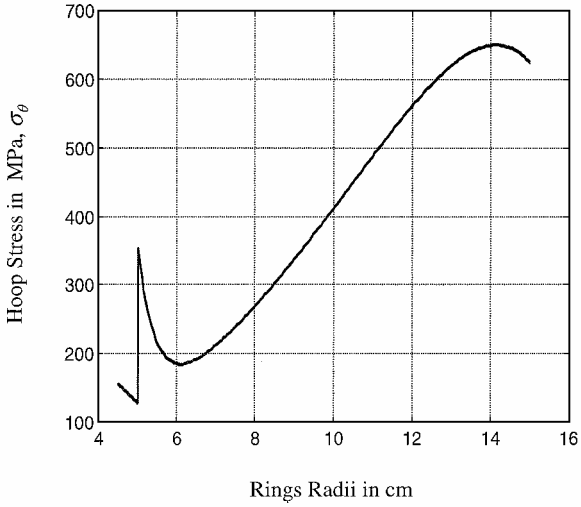

Fig. 13 Hoop stress in optimum solution rotor at 42,735 rpm.

hoop direction. This is because, although the hoop stresses can be decreased by using a $(\pm 20 \text{ deg})_s$ axisymmetric laminated rotor, the accompanying increase in the radial stresses will decrease the FS of the rotor. The contact radius between the steel ring and the GRE ring is 50 mm, and the amount of interference is 0.01 mm. For a total mass of 1.2 kg and for an output maximum momentum of $55 \text{ N} \cdot \text{m} \cdot \text{s}$, the rotor length is 9.275 mm, and the maximum angular velocity is 42,735 rpm. According to the Tsai–Wu failure criterion, the FS associated with those design parameters is 1.33. The hoop stress distribution at this maximum operational speed is shown in Fig. 13.

Note that the mentioned suggested design is only based on the investigation of the deign parameters treated in this paper. However, for a complete thorough design, two important subjects should be given great care in the design process. The first issue is the inclusion of the effect of the process-induced residual stresses in the stress analysis of the rotor. The second subject to be considered in an integrated analysis is the problem of free edge stresses that arise in laminated rings. For a complete treatment of both subjects, see Refs. 16 and 17, respectively.

Conclusions

The mathematical models developed for the isotropic as well as the axisymmetric laminated cases proved that the performance of conventional isotropic steel–aluminum rotors is well below that of the suggested GRE laminated rotors in terms of stiffness and strength. Furthermore, the study shows that the behavior of axisymmetric GRE laminate is different from that of isotropic materials under constant speeds as the only loading condition. For isotropic materials, the hoop stress is maximum at the rotor inner radius, whereas, for laminated material with the fibers aligned in the hoop direction, the hoop stress is maximum at a point close to the outer radius. It was proved that, by changing the lamination angle from 0 to 40 deg, a case close to the isotropic behavior, the hoop stress changed to a distribution close to the isotropic case.

The parametric analysis carried out on the GRE rotor design proved that it is more efficient to use minimum interferences between the neighboring rings, just to keep them in contact while rotating at maximum operating speed. The analysis also proved that there is an inverse relation between the reinforcement volume fraction and the amount of interferences needed to keep the rings in contact while operating at same speeds.

The parametric analysis of axisymmetric laminated GRE rotors also proves that, for such an application, operating at high speeds, the hoop stresses are the dominant factor for failure. Therefore, it is advised to orient all of the fibers in the hoop direction to provide stiffness and strength in this direction. Although the study of the behavior of axisymmetric laminate shows that the lowest hoop stresses, among all five lamination angles studied, occur at a lamination angle of $(\pm 20 \text{ deg})_s$, the associated maximum radial stress in this case increases to more than four times that of the 0-deg lamination angle case. Consequently, the maximum FS can be obtained by using a 0-deg rather than a $(\pm 20 \text{ deg})_s$ laminate for the design of the GRE rotor. Finally, it was determined that, for such an application, it is more advantageous to use a minimum number of rings to minimize maximum hoop stresses. It was found that, although the interferences decrease the hoop stresses of the inner rings, they increase the hoop stresses of the outer ring, which exhibits higher stresses naturally as a result of the centrifugal loading.

Finally, a 1.2-kg two-ring rotor running at 42,735 rpm is suggested for the design of the magnetically suspended FMW rotor. The inner ring is to be made from steel to provide the required interaction with the magnetic bearings and is only 5 mm thick, whereas the outer ring is to be made from 70% GRE with a 0-deg lamination angle. The FS associated with this design is 1.33. In this design, by using a GRE rotor, a 70% reduction in mass was achieved as compared to the original 4-kg aluminum momentum wheel rotor. Usually two fixed momentum wheels are mounted on the pitch axis of commercial satellites for redundancy; therefore, the suggested design offers a 5.6-kg reduction in satellite mass. According to Ref. 18, the cost of launching 1-kg of commercial payload to geosynchronous orbit is about U.S. $30,000/kg. Consequently, the mentioned mass reduction corresponds to U.S. $168,000 (Ref. 18).

Appendix: Differential Operators

$$D_1 u = \frac{\mathrm{d}u}{\mathrm{d}t} \tag{A1}$$

$$D_1 u = \frac{\mathrm{d}u}{\mathrm{d}r}\frac{\mathrm{d}r}{\mathrm{d}t} \tag{A2}$$

$$D_1 u = \frac{\mathrm{d}r}{\mathrm{d}t}\frac{\mathrm{d}u}{\mathrm{d}r} \tag{A3}$$

$$D_1 u = r D u \tag{A4}$$

$$D_1(D_1 - 1)u = D_1^2 - D_1 u \tag{A5}$$

$$D_1(D_1 - 1)u = \frac{\mathrm{d}^2 u}{\mathrm{d}t^2} - \frac{\mathrm{d}u}{\mathrm{d}t} \tag{A6}$$

$$D_1(D_1 - 1)u = \frac{\mathrm{d}}{\mathrm{d}t}\left(\frac{\mathrm{d}u}{\mathrm{d}t}\right) - \frac{\mathrm{d}u}{\mathrm{d}t} \tag{A7}$$

$$D_1(D_1 - 1)u = \frac{\mathrm{d}}{\mathrm{d}t}\left(r\frac{\mathrm{d}u}{\mathrm{d}r}\right) - r\frac{\mathrm{d}u}{\mathrm{d}r} \tag{A8}$$

$$D_1(D_1 - 1)u = \left(r\frac{\mathrm{d}^2 u}{\mathrm{d}r\,\mathrm{d}t} + \frac{\mathrm{d}u}{\mathrm{d}r}\frac{\mathrm{d}r}{\mathrm{d}t}\right) - r\frac{\mathrm{d}u}{\mathrm{d}r} \tag{A9}$$

$$D_1(D_1 - 1)u = r^2 D u\frac{\mathrm{d}u}{\mathrm{d}r} + r\frac{\mathrm{d}u}{\mathrm{d}r} - r\frac{\mathrm{d}u}{\mathrm{d}r} \tag{A10}$$

$$D_1(D_1 - 1)u = r^2 D^2 u \tag{A11}$$

References

[1] Hassan, R., "Analysis of Fiber-Reinforced Laminated Momentum Wheel Rotors," M.Sc. Thesis, Mechanical Engineering Dept., American Univ., Cairo, July 1999.

[2] "Teldix Products and Services, Space Products, Ball Bearing Momentum Wheels, DRALLRAD DR 35," Teldix Co., Heidelberg, Germany, URL: http://www.teldix.com/index.htm [cited July 1999].

[3] "Honeywell Commercial Electromechanical Products, MWAs Product Specification Sheets, Model HM 4520," Honeywell, Inc., Phoenix, AZ, URL: http: // content.honeywell.com/Space/CEM/PDF/heritageRWA / HM4520% 20Tech%20 Sheet.pdf [cited July 1999].

[4] Akishita, S., Tsuchiya, K., Nakajima, A., and Murakami, C., "Anisotropic Stiffness Effect on Stability of a Magnetically Suspended Momentum Wheel," *Journal of Guidance, Control, and Dynamics*, Vol. 14, No. 2, 1991, pp. 330–336.

[5] Kirk, J. A., Jayaraman, C. P., Anand, D. K., and Anjanappa, M., "Rotor Dynamics of Flywheel Energy Storage System," *Journal of Solar Energy Engineering*, Vol. 113, No. 1, 1991, pp. 11–18.

[6]Wertz, J., and Larson, W. (eds.), *Space Mission Analysis and Design*, 3rd ed., Microcosm, Torrance, CA, 1999, pp. 332–335.

[7]Pawlik, P. S., and Reismann, H., *Elasticity: Theory and Applications*, 1st ed., Wiley, New York, 1980, pp. 65–118.

[8]Hassan, R., Younan, M., Arafa, H., and Bahei-El-Din, Y., "Analysis of Axi-nonsymmetric Laminated Rings for the Design of Momentum Wheel Rotors," *Mechanics and Materials in Design 2000, 3rd International Conference*, Univ. of Toronto Press, Toronto, ON, Canada, 2000, pp. 11–22.

[9]Mori, T., and Tanaka, K., "Average Stress in Matrix and Average Elastic Energy of Materials with Misfitting Inclusions," *Acta Metallurgica*, Vol. 21, No. 5, 1973, pp. 571–574.

[10]Jones, R. M., *Mechanics of Composite Materials*, 1st ed., McGraw–Hill, New York, 1975, pp. 147–172.

[11]Farag, M. M., *Selection of Materials and Manufacturing Processes for Engineering Design*, 1st ed., Prentice–Hall, Upper Saddle River, NJ, 1989, pp. 324–339.

[12]Bahei-El-Din, Y. A., Dvorak, G. J., and Wu, J. F., "Dimensional Stability of Metal-Matrix Laminates," *Journal of Composite Sciences and Technology*, Vol. 43, No. 3, 1992, pp. 207–219.

[13]Jeong, H. M., Ha, S. K., and Cho, Y. S., "Optimum Design of Thick-Walled Composite Rings for an Energy Storage System," *Journal of Composite Materials*, Vol. 32, No. 9, 1998, pp. 851–873.

[14]Tutuncu, N., "Intralaminar Failure Stresses Due to Centrifugal Forces in Polar-Anisotropic Circular Plates," *Journal of Composite Materials*, Vol. 32, No. 21, 1998, pp. 1948–1963.

[15]Kirk, J. A., "Flywheel Energy Storage-I: Basic Concepts," *Journal of Mechanical Engineering Science*, Vol. 19, No. 4, 1977, pp. 223–231.

[16]Gabrys, C. W., and Bakis, C. E., "Simplified Analysis of Residual Stresses in In-Situ Cured Hoop-Wound Rings," *Journal of Composite Materials*, Vol. 32, No. 13, 1998, pp. 1325–1343.

[17]Herakovich, C. T., "Edge Effects and Delamination Failures," *Journal of Strain Analysis*, Vol. 24, No. 4, 1989, pp. 245–252.

[18]Ashley, S., "Bringing Launch Costs Down to Earth," *Mechanical Engineering*, Vol. 120, No. 10, 1998, pp. 62–68.

R. B. Malla
Associate Editor